# Geophysical Research Letters®

**Key Points:**

- Stratospheric Aerosol Injection (SAI) impacts the Southern Annular Mode (SAM), and the response is strongly sensitive to the latitude of SAI
- Injections in the Northern Hemisphere drive positive SAM response and injections in the Southern Hemisphere drive negative SAM response
- Meridional extent of lower stratospheric aerosol heating likely an important contributor to the sensitivity to injection latitude

**Supporting Information:**

Supporting Information may be found in the online version of this article.

**Correspondence to:**

E. M. Bednarz,
ewa.bednarz@cornell.edu

# Impact of the Latitude of Stratospheric Aerosol Injection on the Southern Annular Mode

**Ewa M. Bednarz[1]** , **Daniele Visioni[1]** , **Jadwiga H. Richter[2]** , **Amy H. Butler[3]** , **and Douglas G. MacMartin[1]**

[1]Sibley School of Mechanical and Aerospace Engineering, Cornell University, Ithaca, NY, USA, [2]National Center for Atmospheric Research, Climate and Global Dynamics Laboratory, Boulder, CO, USA, [3]National Oceanic and Atmospheric Administration, Chemical Sciences Laboratory, Boulder, CO, USA

**Abstract** The impacts of Stratospheric Aerosol Injection (SAI) strategies on the Southern Annular Mode (SAM) are analyzed with the Community Earth System Model. Using a set of simulations with fixed single-point $SO_2$ injections we demonstrate the first-order dependence of the SAM response on the latitude of injection, with the northern hemispheric and equatorial injections driving a response corresponding to a positive phase of SAM and the southern hemispheric injections driving a negative phase of SAM. We further demonstrate that the results can to first order explain the differences in the SAM responses diagnosed from the two recent large ensembles of geoengineering simulations utilizing more complex injection strategies – Geoengineering Large Ensemble and Assessing Responses and Impacts of Solar climate intervention on the Earth system with Stratospheric Aerosol Injection (GLENS and ARISE-SAI) – as driven by the differences in the simulated sulfate aerosol distributions. Our results point to the meridional extent of aerosol-induced lower stratospheric heating as an important driver of the sensitivity of the SAM response to the injection location.

**Plain Language Summary** Stratospheric Aerosol Injection (SAI) is a proposed climate intervention method in which sulfate aerosol precursors are injected into the lower stratosphere to mitigate some of the negative impacts of climate change. Here we analyze SAI impact on the Southern Annular Mode (SAM), a dominant mode of interannual climate variability in the southern mid- and high latitudes, using the Community Earth System Model. Using a set of simulations with fixed single-point injections of aerosol precursors we demonstrate the first-order dependence of the SAM response on the latitude of injection, with the northern hemispheric and equatorial injections driving a response corresponding to a positive phase of SAM and the southern hemispheric injections driving a negative phase of SAM. We further demonstrate that our results can to first order explain the differences in the SAM responses diagnosed from the two recent large ensembles of geoengineering simulations utilizing more complex injection strategies as driven by the differences in the simulated sulfate aerosol distributions. Our findings illustrate the complex interplay of the microphysical, radiative and dynamical processes contributing to the SAI responses on regional scales.

## 1. Introduction

Stratospheric Aerosol Injection (SAI) is a stopgap measure proposed to mitigate some of the negative impacts of rising greenhouse gas (GHG) levels by reducing surface temperatures through the injection of aerosol precursors into the stratosphere. Yet, despite offsetting global mean surface temperature, various studies demonstrated that SAI would also alter atmospheric circulation in a manner different to that arising from the climate change alone, thereby potentially playing an important role in modulating regional and seasonal climate variability (e.g., Banerjee et al., 2021; Simpson et al., 2019). Recent studies showed that warming in the tropical lower stratosphere brought about by the absorption of solar and terrestrial radiation by sulfate aerosols can drive a strengthening of the stratospheric polar vortex in the Northern Hemisphere during winter (e.g., Banerjee et al., 2021; Ferraro et al., 2015; Jones et al., 2022). The response manifests at the surface as a positive phase of the Northern Annular Mode (NAM), for the Atlantic sector only known also as the North Atlantic Oscillation, with consequences for winter surface temperatures and precipitation patterns in Europe and North America (Thompson & Wallace, 1998).

Potential SAI impacts on the Southern Hemisphere (SH) counterpart - the Southern Annular Mode (SAM), also known as the Antarctic Oscillation - have not, however, so far received much attention. The SAM is the dominant

mode of SH high-latitude climate variability (Thompson & Wallace, 2000). Its changes have been extensively studied for instance in the context of climate impacts from rising GHG emissions and from stratospheric ozone depletion and recovery (e.g., Banerjee et al., 2020; McLandress et al., 2011; Polvani et al., 2011; Son et al., 2009), and its associated impacts on temperature and precipitation patterns over much of the SH (Kang et al., 2011). Regarding impacts from a potential SAI scenario, McCusker et al. (2015) found that the presence of sulfate aerosols in the tropical lower stratosphere drives strengthening of the SH polar vortex that extends down to the surface. More recently, Bednarz, Visioni, Banerjee, et al. (2022) showed that the signature of the equatorial sulfate injection corresponds to a poleward shift of the SH tropospheric eddy-driven jet and a pattern of sea-level pressure changes resembling the positive phase of SAM.

Importantly, most of the assessments of dynamical signatures of potential geoengineering scenarios come from climate model simulations in which $SO_2$ is injected in the lower stratosphere in the equatorial or tropical region (i.e., 10°S–10°N). While the choice of injection location could lead to different climate impacts (see e.g., Kravitz et al., 2019), a detailed assessment of the role of the injection location for the simulated stratospheric dynamical response has so far been missing. Recently, Visioni et al. (2022) and Bednarz, Visioni, Kravitz, et al. (2022) analyzed sources of uncertainty in model projections of the atmospheric and surface climate responses to fixed annual single-point $SO_2$ injections at either 30°S, 15°S, 0°, 15°N or 30°N simulated in three comprehensive Earth System Models (ESMs). However, the relatively short length of simulations (10 years) presented challenges in confident assessment of the associated dynamical responses. Here we extend the original 10-year long CESM2-WACCM6 integrations into two 35-year-long ensemble members; the longer simulations allow us to better isolate the impacts of SAI on atmospheric circulation and the underlying physical mechanisms. We analyze the resulting impacts on the SAM, focusing on the dependence on the latitude of $SO_2$ injection. We then discuss the SH high latitude signature of SAI simulated in two recent large SAI ensembles, the Geoengineering Large Ensemble (GLENS, Tilmes et al., 2018) and the Assessing Responses and Impacts of Solar climate intervention on the Earth system with Stratospheric Aerosol Injection (ARISE-SAI, Richter et al., 2022). By doing so, we demonstrate that our fixed injection results largely explain the differences in the SAM responses simulated in these two experiments, thus providing further evidence for the role of the sulfate aerosol distribution for determining the SH dynamical response.

## 2. Methods

### 2.1. Single-Point Injection Runs

We use version 2 of the Community Earth System Model (CESM) coupled to version 6 of the Whole Atmosphere Community Climate Model, CESM2-WACCM6 (Danabasoglu et al., 2020; Gettelman et al., 2019). The horizontal resolution is 1.25° longitude by 0.9° latitude, with 70 vertical levels up to ~130 km. The model is run in the Middle Atmosphere configuration, including comprehensive interactive stratospheric and upper atmospheric chemistry as well as interactive aerosol microphysics using the Modal Aerosol Module (MAM4; Liu et al., 2016).

We perform five sensitivity experiments under background CMIP6 SSP2-4.5 GHG scenario (Meinshausen et al., 2020) with fixed single-point 12 Tg-$SO_2$/yr injections at 22 km in altitude and either 30°S, 15°S, 0°, 15°N, or 30°N longitude. Each experiment consists of two ensemble members initialized in January 2035 and extending up to the end of 2069. The detailed experimental protocol as well as the results of the initial 10 years of each first ensemble member are described in Visioni et al. (2022) and Bednarz, Visioni, Kravitz, et al. (2022). Here we analyze the results from the last 20 years of the simulations (i.e., 2050–2069) and compare them against the baseline reference period chosen as the 2020–2039 mean of the corresponding control SSP2-4.5 experiment without SAI (mean over the three ensemble members available).

### 2.2. Large SAI Ensembles

We use two recent large CESM SAI ensembles - GLENS (Tilmes et al., 2018) and ARISE-SAI (Richter et al., 2022). In both cases, $SO_2$ was injected into the lower stratosphere at four off-equatorial locations – 30°S, 15°S, 15°N, and 30°N – using a feedback algorithm that controls the injection amount at each latitude with the aim to maintain the global mean surface temperature and its equator-to-pole and inter-hemispheric gradients at the baseline levels (Kravitz et al., 2017; MacMartin et al., 2017).

GLENS was carried out using CESM1(WACCM) under high-end Representative Concentration Pathway 8.5 (RCP8.5; Fujino et al., 2006; Hijioka et al., 2008) GHG scenario. $SO_2$ was injected 7 km above the tropopause at

each of the four latitudes starting in the year 2020 and continuing until the end of the century. The baseline chosen for the feedback algorithm was the 2010–2030 mean.

ARISE-SAI was carried out using CESM2-WACCM6 under the moderate SSP2-4.5 (Meinshausen et al., 2020) GHG scenario. $SO_2$ was injected at 22 km (at all latitudes) starting in the year 2035 and extending to the year 2069. The baseline chosen for the feedback algorithm was the 2020–2039 mean, corresponding to the likely period when the real world will reach 1.5 K above pre-industrial conditions (MacMartin et al., 2022; Tebaldi et al., 2021).

For ARISE-SAI, we analyze the responses over the last 20 years of the simulations (2050–2069), where a cooling of 0.88 K on average is necessary to keep the temperatures at the baseline level. For GLENS, we analyze the responses over two periods: the end of the century (2070–2089), which maximizes the amplitude of the response as well as the fraction of the $SO_2$ injections occurring in the NH (Tilmes et al., 2018), and the mid-century (2038–2057), where the same amount of cooling is reached compared to baseline as for ARISE-SAI in 2050–2069 (Figure S1 in Supporting Information S1).

## 3. SAM Response in the Single-Point Injection Experiments

Figure 1 (left panels) shows sulfate aerosol concentrations simulated in each of the fixed injection experiments. As expected, the largest aerosol concentrations are found in the lower stratosphere near the $SO_2$ injection location. However, significant levels of aerosols are also found at higher latitudes for all off-equatorial injection cases, as the aerosols formed from the $SO_2$ oxidation and subsequent nucleation or coagulation are transported poleward by the shallow branch of the Brewer-Dobson circulation.

The absorption of solar and terrestrial radiation by sulfate increases temperatures in the tropical lower stratosphere (right panels in Figure 1). For the off-equatorial injections, the warming extends also to the mid-latitude and subpolar regions, consistent with the presence of elevated aerosol levels. These lower stratospheric temperature changes modulate meridional temperature gradients, which are directly related to the vertical shear of zonal wind and can thus initiate a dynamical response at higher latitudes. We note that the direct radiative effect of SAI on lower stratospheric temperatures is difficult to fully isolate in our experiments because the temperature response includes not only the aerosol heating but also temperature changes caused by the dynamical response to SAI (see below), as well as radiative effects due to long-term changes in GHGs and ozone-depleting substances.

In the SH, we find that all single-point SAI simulations show a strengthening of the Antarctic stratospheric polar vortex (Figure 2, column 1), consistent with the strengthened meridional temperature gradient induced by aerosol heating. In the troposphere, however, we find different behavior of the zonal winds depending on the latitude of $SO_2$ injection. For the NH and equatorial injections, the stratospheric westerly response extends down to the troposphere at ~60°S, where it is accompanied by an easterly response in the mid-latitudes. These tropospheric zonal wind changes reflect a poleward shift of the eddy-driven jet. At the surface, this corresponds to a decrease in sea-level pressure over Antarctica and an increase in sea-level pressure in the mid-latitude/subpolar regions (column 2 in Figure 2). Such pattern of sea-level pressure anomalies corresponds to the positive phase of SAM and, similarly as the stratospheric and tropospheric zonal wind anomalies, is evident year-round (see Figure S2 in Supporting Information S1 for seasonal zonal wind responses). Importantly, when sulfate precursors are injected in the SH the strengthening of the stratospheric jet does not extend down to the troposphere. Instead, the tropospheric westerly zonal winds weaken at ~60°S and strengthen in the mid-latitudes; this corresponds to the equatorward shift of the eddy-driven jet. At the surface, we thus find a year-round increase in sea-level pressure at the SH high latitudes and a decrease in the mid-latitudes, which corresponds to a negative phase of the SAM.

A number of factors contribute to this simulated dynamical behavior. First, as mentioned above the meridional distribution of sulfate aerosols and the associated heating from aerosol absorption results in different modulations of meridional temperature gradients. Our results suggest that the direct influence of this heating on the tropospheric eddy fluxes is an important driver of the sensitivity of the SAM response to injection location. In idealized experiments, the location of the anomalous lower stratospheric heating was shown to play a first-order role in determining the sign of the tropospheric jet shift in idealized models (e.g., Haigh et al., 2005; Lorenz & DeWeaver, 2007; Simpson et al., 2009). For instance, Haigh et al. (2005) showed that heating in the tropical lower stratosphere leads to a poleward tropospheric jet shift while the shift is equatorward if the heating is imposed in the lower stratosphere uniformly or only at high latitudes. Similar results were also found from experiments
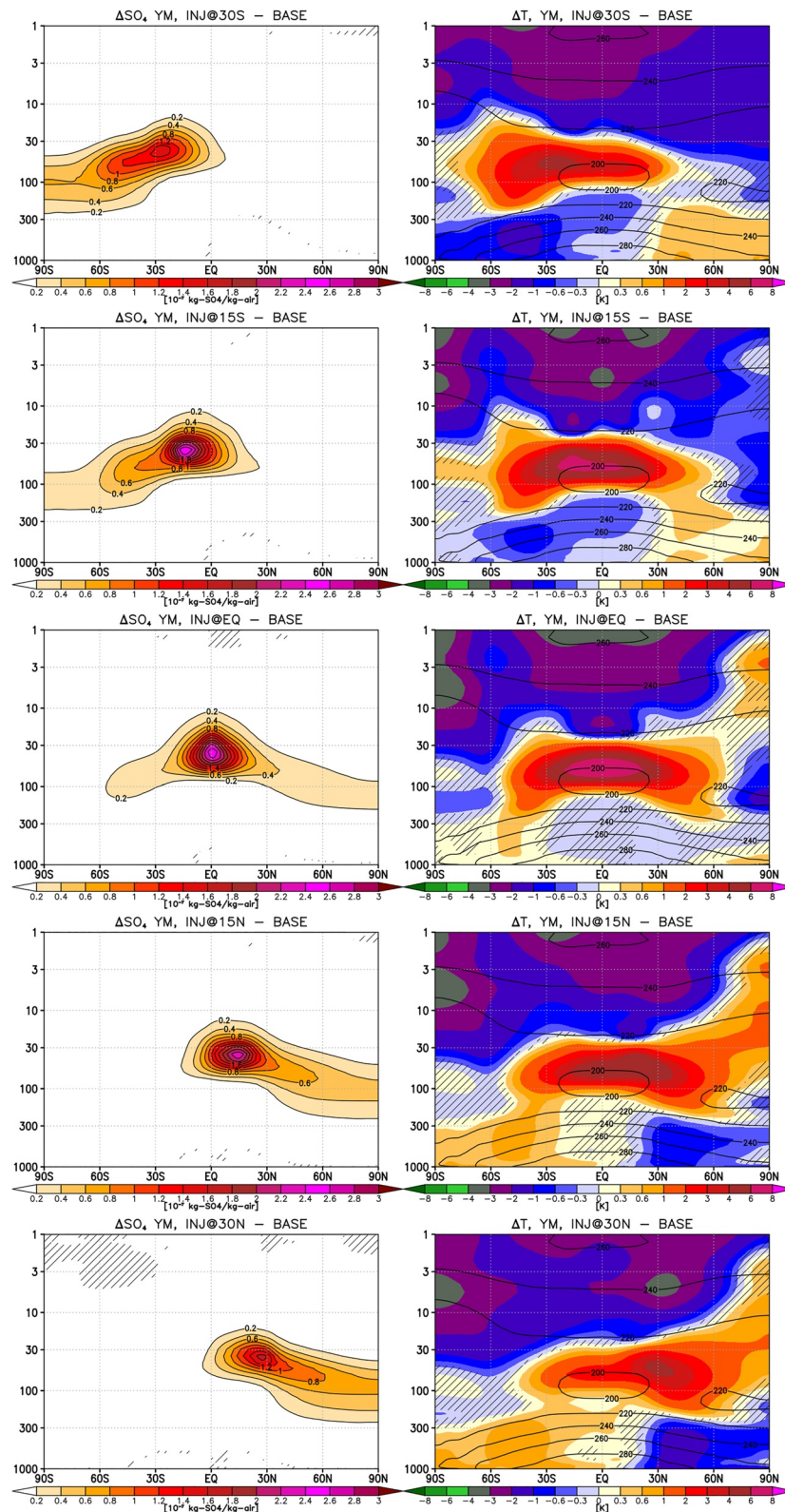
**Figure 1.** Column 1: Yearly mean difference in the simulated sulfate aerosol mass mixing ratio ($10^{-7}$ kg-$SO_4$/kg-air) in each single-point stratospheric aerosol injection (SAI) experiment and the baseline. Column 2: Shading shows the difference in temperature (K) between each of the single-point SAI simulations and the baseline. Contours in column 2 show the corresponding temperatures in the baseline for reference. Hatching indicates the regions where the difference is not statistically significant (here assumed as smaller than $\pm 2$ standard errors).
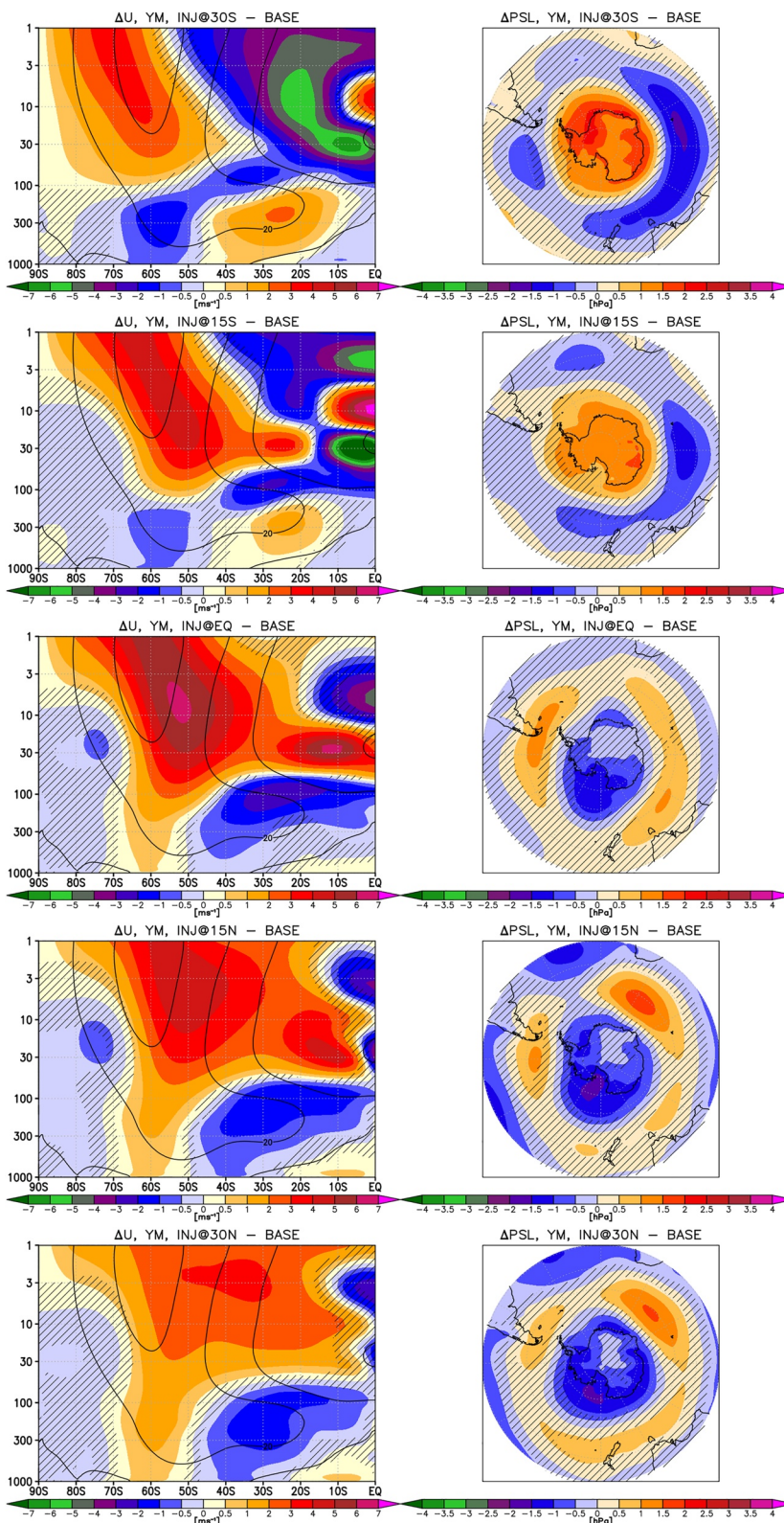
**Figure 2.** Shading: Yearly mean difference in zonal wind (column 1; m/s) and sea-level pressure (column 2; hPa; plotted for the latitudes southward from 30°S) between each of the single-point stratospheric aerosol injection simulations and the baseline. Contours in the left panels indicate the corresponding values in the baseline for reference. Hatching in all plots indicates regions where the response is not statistically significant (±2 standard errors).

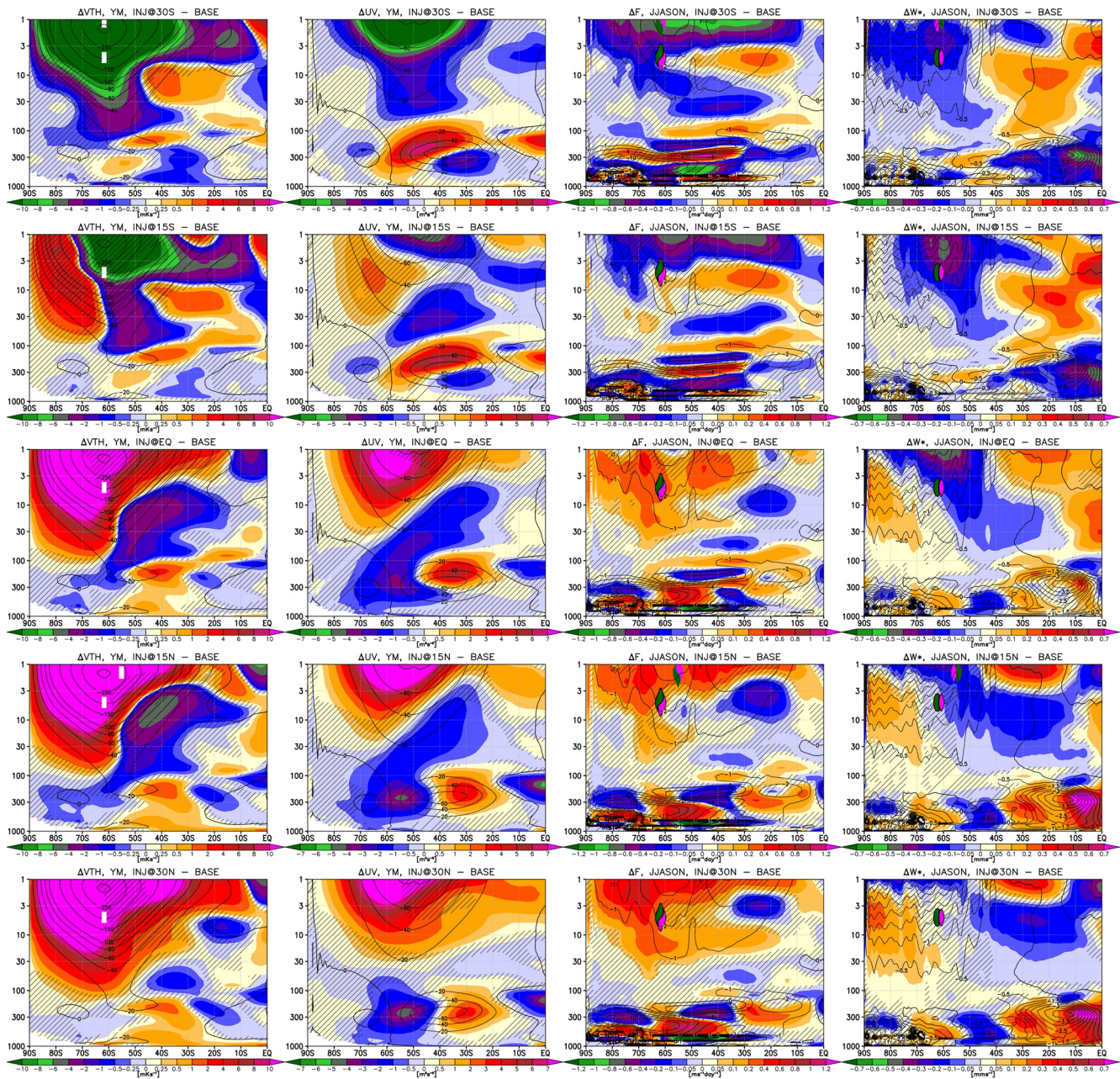**Figure 3.** Shading: Difference in yearly mean northward eddy heat flux $\overline{V'\theta'}$ (column 1; m • K/s), yearly mean northward eddy momentum flux $\overline{U'V'}$ (column 2; m²/s²), June-to-November mean EP flux divergence $\nabla\overline{F}$ (column 3; m/s/day), and June-to-November mean vertical component of the residual circulation, $\overline{w*}$ (column 4; mm/s; positive values indicate upwelling) between each of the single-point stratospheric aerosol injection simulations and the baseline. Contours indicate the corresponding values in the baseline for reference. Hatching indicates regions where the response is not statistically significant (±2 standard errors).

applying anomalous heating in the upper troposphere (e.g., Butler et al., 2010) or throughout the tropospheric column (Baker et al., 2017). Here, the enhanced heating under SH injections extends to near the poleward node of the eddy-driven jet (Figure 1, column 2). This flattens the isentropics in that region (Butler et al., 2011) and shifts the region of strongest isentropic slope (or eddy heat flux; Figure 3 column 1), eddy momentum flux (Figure 3, column 2) and tropospheric eddy-driven jet (Figure 2, column 1) equatorward (cf. Figure 9 in Baker et al., 2017). The opposite is true for the NH injections, where the effect of aerosol heating on the isentropic slope in the SH is shifted toward the subtropics, equatorward of the eddy-driven jet, which instead shifts the tropospheric eddy heat and momentum fluxes poleward.

Notably, there are also changes in tropospheric temperatures brought about by the reduction of incoming solar radiation by sulfate aerosols. As shown in Figure 1 (column 2), the SH $SO_2$ injections lead to tropospheric cooling primarily in the southern mid- and high latitudes relative to present-day conditions. Correspondingly, the NH injections result in tropospheric cooling primarily in that hemisphere, while the southern tropospheric temperatures increase in mid- and high latitudes (as the increase in the radiative forcing from GHGs is not offset by the reduction in incoming solar radiation). In all cases, the tropospheric temperature response is strongest in the mid-latitudes, consistent with the associated shifts of eddy-driven jets under altered meridional temperature gradients between the tropics and mid-latitudes, and between the mid- and high latitudes. We note that, as with the lower stratospheric changes discussed above, the direct radiative impact of SAI on tropospheric temperatures is difficult to isolate here as the temperature response is also modulated indirectly by the dynamical response to SAI itself.

Changes in lower tropospheric temperature gradients drive changes in meridional heat fluxes. Strengthening of the SH tropospheric temperature gradient between the tropics and mid-latitudes under SH injections broadly increases poleward eddy heat flux in the southern subtropical to mid-latitude troposphere, while the opposite is true under the NH injections (Figure 3, column 1). The increased (decreased) meridional heat flux under SH (NH) $SO_2$ injections constitutes an increased (decreased) tropospheric source of wave activity into the stratosphere, which may contribute to the enhanced (reduced) propagation of waves in the stratosphere (see Figure S3 in Supporting Information S1).

In addition, in the stratosphere meridional distribution of sulfate aerosols modulates the location and strength of the maximum meridional temperature gradient. This process controls the thermal wind response. In all experiments, the lower stratospheric temperature gradient in the SH is enhanced, leading to an increase in westerly wind shear in the stratosphere, though the specific latitudes where this occurs varies depending on the injection location. For instance, under injection at 30°S (30°N), the strengthening of the stratospheric zonal wind occurs primarily on the poleward (equatorward) flank of the polar vortex (Figure 2, column 1). Changes in the strength of the stratospheric mean flow can further modulate stratospheric wave propagation and breaking. Since planetary wave propagation requires the background circulation to be westerly (Charney & Drazin, 1961), we focus here on changes during austral winter and spring (June to November, JJASON). The enhanced propagation and breaking of planetary-scale waves in the southern stratosphere under SH $SO_2$ injections is illustrated by the increase in Eliassen-Palm flux (EP flux, see e.g., Andrews et al., 1987) convergence in Figure 3 (column 3). The opposite is true for the NH injections which show reduced wave propagation and breaking (increase in EP flux divergence in Figure 3). The changes in wave propagation under SH (NH) injections are associated with increased (decreased) high latitude downwelling (column 4 in Figure 3), and increased (decreased) adiabatic warming. This modulation of the waves can modulate the stratospheric vortex response expected due to thermal wind alone. The stratospheric response can couple downwards to the troposphere through wave-mean flow interactions and eddy feedbacks. During austral spring and summer, when stratosphere-troposphere coupling occurs, this can thus act to amplify the equatorward (poleward) shift of the tropospheric jet stream for SH (NH) injections.

We note that all of these processes are inherently connected. Further idealized experiments would thus be needed to decouple the various processes and to identify the dominant drivers of the contrasting responses of the SH high latitude circulation and surface climate to the different SAI locations. The year-round character of the response points to the dominant role of the eddy heat and momentum fluxes within the troposphere caused by the changes in the meridional temperature gradients in the lower stratosphere and the troposphere below, rather than to the dynamical top-down influence from the stratosphere on its own (which is more seasonal in character). Nonetheless, the later can constitute a plausible contributing factor in austral spring.

Similar impacts of SAI on SAM are diagnosed from the simulations if the results are compared against the corresponding control SSP2-4.5 experiment using the same time period (Figures S4–S5 in Supporting Information S1); this further confirms that the diagnosed SAM impacts arise from SAI, and the differences in SAI locations, rather than from climate change alone. We note that our results could be model dependent and, thus, future studies should investigate this with other climate models.

## 4. SAM Response in the Large SAI Ensembles

Having discussed the SH high latitude response to the constant single-point $SO_2$ injections to understand the dependence on the latitude of injection, we now analyze the analogous SAM responses in the two large CESM
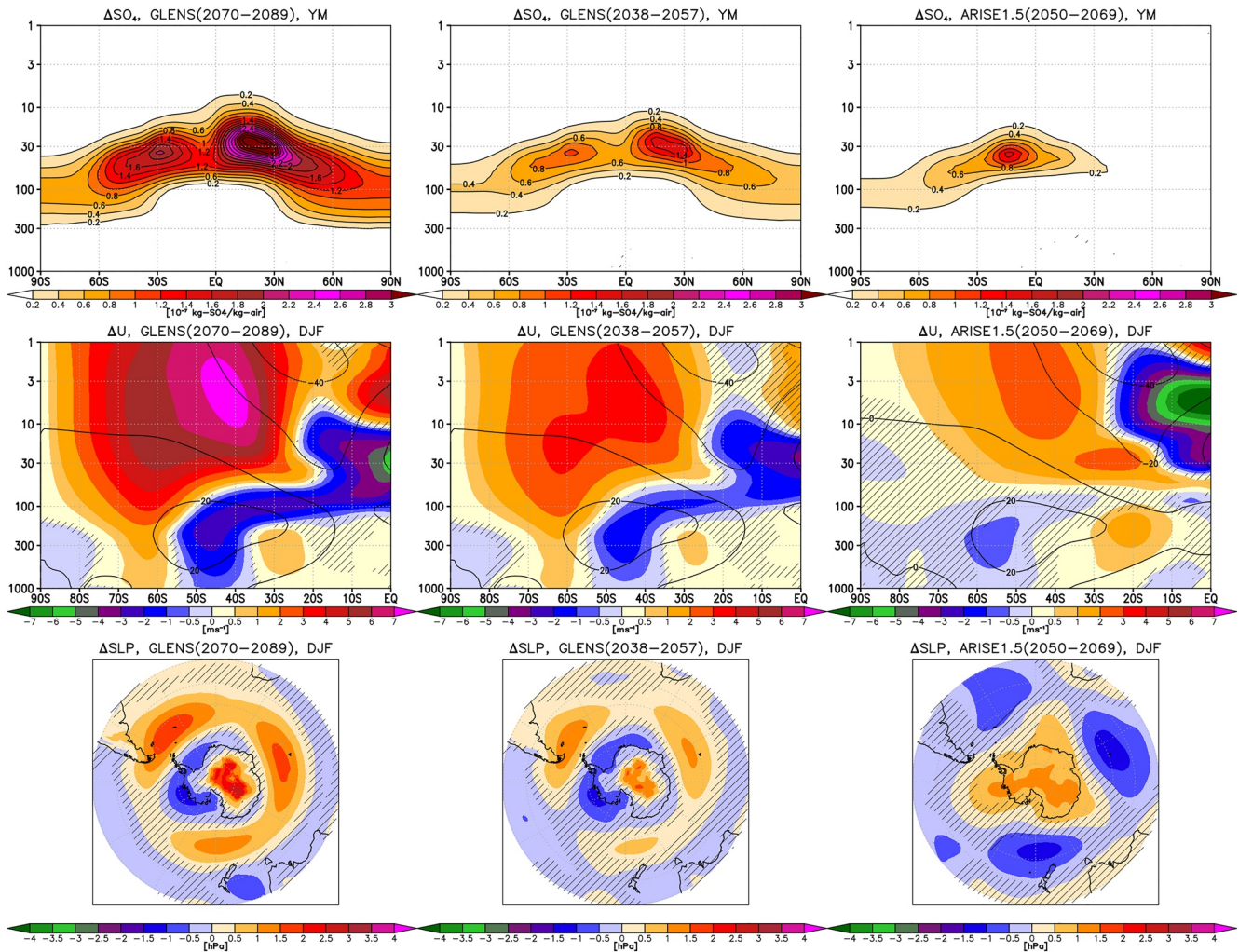
**Figure 4.** Shading: Changes in the yearly mean sulfate aerosol mass mixing ratios ($10^{-7}$ kg-$SO_4$/kg-air; top), DJF zonal wind in the southern hemisphere (m/s; middle), and DJF sea level pressure southward of 30°S (hPa, bottom) compared to the respective baseline periods (here chosen as 2011–2030 and 2020–2039 for Geoengineering Large Ensemble (GLENS) and Assessing Responses and Impacts of Solar climate intervention on the Earth system with Stratospheric Aerosol Injection (ARISE-SAI), respectively). Column 1 is for GLENS averaged over 2070–2089, column 2 is for GLENS averaged over 2038–2057, column 3 is for ARISE-SAI averaged over 2050–2069. Contours in row 2 indicate the corresponding baseline values for reference.

SAI ensembles utilizing more complex SAI strategies. In particular, both GLENS and ARISE-SAI injected $SO_2$ at four off-equatorial locations using a feedback algorithm that aims to maintain the global mean surface temperatures and their equator-to-pole and inter-hemispheric gradients at the baseline levels. The two ensembles utilized two different GHG emission scenarios - RCP8.5 and SSP2-4.5, respectively – resulting in different total magnitudes of the injections (Richter et al., 2022). Furthermore, the distribution of the $SO_2$ injections across the four latitudes differed significantly between the two ensembles (Fasullo & Richter, 2022), resulting in contrasting distributions of the sulfate aerosols simulated in the stratosphere (Figure 4, top panels). GLENS shows the largest concentrations of sulfate in the NH tropics, in particular for the end of the century. In contrast, the aerosol cloud in ARISE-SAI maximizes in the SH tropics, consistent with the largest injection rates at 15°S (Richter et al., 2022). The underlying reasons behind the change in the dominant injection locations between the two ensembles is investigated in Fasullo and Richter (2022).

Both GLENS and ARISE-SAI show year-round strengthening of the SH stratospheric zonal winds under SAI compared to their baseline periods (Figure S6 in Supporting Information S1). The GLENS westerly response is stronger than in ARISE-SAI, in particular for the end of the century (2070–2089) but also for the mid-century period (2038–2057, i.e., when a similar level of cooling is reached in GLENS to that in the last 20 years of

ARISE-SAI, see Section 2). This is commensurate with the larger injection rates needed in GLENS both to offset the end of the century RCP8.5 GHG scenario (38 Tg-$SO_2$/yr over 2070–2089) or to reach the same amount of global cooling (15 Tg-$SO_2$/yr over 2038–2057) as in ARISE-SAI (10 Tg-$SO_2$/yr over 2050–2069).

Despite the qualitative similarities in the SH stratospheric zonal wind responses between GLENS and ARISE-SAI, contrastingly different impacts are found in the troposphere. We choose to focus here on the austral summer (DJF, rows 2–3 in Figure 4), that is, when the tropospheric response is particularly clear, although overall similar results are also found if the yearly mean data is considered instead (Figure S6 in Supporting Information S1). In GLENS, the strengthening of the stratospheric zonal winds extends down to the troposphere, resulting in a poleward shift of the eddy-driven jet and sea-level pressure anomalies corresponding to the positive phase of SAM. The tropospheric GLENS responses are qualitatively similar for both the end of the century (left columns in Figure 4 and Figure S6 in Supporting Information S1) and mid-century (middle columns in Figure 4 and Figure S6 in Supporting Information S1) periods. In contrast, an opposite sign tropospheric response is found in ARISE-SAI (right columns in Figure 4 and Figure S6 in Supporting Information S1), that is, an equatorward shift of the eddy-driven jet and a sea-level pressure response resembling a negative phase of SAM. We note that the yearly mean Antarctic polar vortex response in ARISE-SAI is largely not symmetrical, and thus both zonal wind and sea-level responses become diminished when averaged over all longitudes (Figure S6 in Supporting Information S1, right column). A more symmetric response is found during austral summer (Figure 4, right column).

The differences between the tropospheric zonal wind and sea-level pressure responses to SAI between the two large SAI ensembles agree with the results of the fixed single-point injection simulations. In particular, the SAI impacts on SAM in GLENS, where the largest sulfate concentrations are found in the NH tropics, qualitatively agree with the results of the fixed NH $SO_2$ injection simulations. The SAI impacts on SAM found in ARISE-SAI, on the other hand, where the largest aerosol concentrations are found in the SH tropics, qualitatively agree with the results of the fixed SH $SO_2$ injection simulations.

Our results thus demonstrate that the differences in the SAI impacts on the SH high latitude climate simulated by these two large ensembles can be explained by the corresponding differences in the sulfate aerosol distributions. We note that other potential drivers of the differences in the SAI responses between GLENS and ARISE-SAI exist, for instance inter-model differences between CESM1(WACCM) and CESM2-WACCM6 models or the different spatial and temporal patterns of the radiative forcings in RCP8.5 and SSP2-4.5 scenarios (Fasullo & Richter, 2022). Yet, the results of our idealized runs with fixed single-latitude injections point strongly to the dominant role of sulfate distributions in driving the different SAM impacts in the CESM model.

## 5. Summary and Discussion

Numerous modeling studies in the past investigated impacts of potential SAI on atmospheric circulation, with particular attention given to the impacts on the NH winter polar vortex and the NAM. Yet, potential impacts on its SH counterpart, the SAM, have so far received less attention. Here we analyzed the impacts of SAI on SAM using a number of simulations carried out with the CESM model, and demonstrated the first-order dependence of the simulated SH high latitude response on the latitude of injection.

First, we analyzed the results of a set of runs with fixed annual $SO_2$ injections in the lower stratosphere at either 30°S, 15°S, 0°, 15°N or 30°N. All simulations showed year-round strengthening of the SH stratospheric polar vortex, consistent with overall strengthened horizontal temperature gradients from aerosol heating in the tropical lower stratosphere. However, for the equatorial and NH $SO_2$ injection simulations, the year-round tropospheric circulation response is a poleward shift of the eddy-driven jet with a corresponding pattern of sea-level pressure changes projecting on the positive phase of SAM. In contrast, in the SH $SO_2$ injections the tropospheric jet shifts equatorward and the sea-levels pressure changes project on the negative phase of SAM. These contrasting responses are associated with consistent changes in eddy heat and momentum fluxes within the troposphere, as well as with changes in stratospheric wave propagation/breaking and the high latitude downwelling during austral winter and spring. We then demonstrated that the results of the single-point injections explain the differences in the SAM responses diagnosed from the two large CESM SAI ensembles utilizing more complex SAI strategies – GLENS and ARISE-SAI. In particular, the predominantly NH-distributed sulfate aerosols in GLENS led to the poleward shift of the SH eddy-driven jet and the positive phase of SAM. In contrast, the predominantly SH-distributed aerosols in ARISE-SAI resulted in the equatorward shift of the SH eddy-driven jet and the negative SAM phase.

The results highlight the dominant role of horizontal sulfate aerosol distribution in driving the different SAM impacts from geoengineering simulations in the CESM model. Our results point to the importance of the meridional distribution of the aerosol-induced lower stratospheric heating as an important driver of the sensitivity of the SAM response to injection location. However, further idealized studies would be needed to decouple the different radiative and dynamical processes operating and influencing stratospheric-tropospheric coupling and, thus, to quantify the relative importance of the various drivers. Our findings illustrate and highlight the complex interplay of the microphysical, radiative and dynamical processes contributing to the SAI responses on regional scales.

## Conflict of Interest

The authors declare no conflicts of interest relevant to this study.

## Data Availability Statement

Data from the community Earth system model (CESM) fixed single point simulations used in this manuscript are available from the Cornell eCommons repository under https://doi.org/10.7298/y8jq-tm62. Geoengineering large ensemble (GLENS) data is available from https://doi.org/10.5065/D6JH3JXX. Assessing responses and impacts of solar climate intervention on the Earth system with stratospheric aerosol injection (ARISE-SAI) data is available from https://doi.org/10.5065/9kcn-9y79.

## References

Andrews, D. G., Holton, J. R., & Leovy, C. B. (1987). *Middle atmosphere dynamics* (p. 489). Academic Press.

Baker, H. S., Woollings, T., & Mbengue, C. (2017). Eddy-driven jet sensitivity to diabatic heating in an idealized GCM. *Journal of Climate*, *30*(16), 6413–6431. https://doi.org/10.1175/jcli-d-16-0864.1

Banerjee, A., Butler, A. H., Polvani, L. M., Robock, A., Simpson, I. R., & Sun, L. (2021). Robust winter warming over Eurasia under stratospheric sulfate geoengineering – The role of stratospheric dynamics. *Atmospheric Chemistry and Physics*, *21*(9), 6985–6997. https://doi.org/10.5194/acp-21-6985-2021

Banerjee, A., Fyfe, J. C., Polvani, L. M., Waugh, D., & Chang, K. L. (2020). A pause in Southern Hemisphere circulation trends due to the Montreal Protocol. *Nature*, *579*(7800), 544–548. https://doi.org/10.1038/s41586-020-2120-4

Bednarz, E. M., Visioni, D., Banerjee, A., Braesicke, P., Kravitz, B., & MacMartin, D. G. (2022). The overlooked role of the stratosphere under a solar constant reduction. *Geophysical Research Letters*, *49*(12). https://doi.org/10.1029/2022GL098773

Bednarz, E. M., Visioni, D., Kravitz, B., Jones, A., Haywood, J. M., Richter, J., et al. (2022). Climate response to off-equatorial stratospheric sulfur injections in three Earth system models – Part 2: Stratospheric and free-tropospheric response. Atmospheric Chemistry and Physics Discussions [preprint]. https://doi.org/10.5194/acp-2022-372

Butler, A. H., Thompson, D. W. J., & Birner, T. (2011). Isentropic slopes, downgradient eddy fluxes, and the extratropical atmospheric circulation response to tropical tropospheric heating. *Journal of the Atmospheric Sciences*, *68*(10), 2292–2305. https://doi.org/10.1175/jas-d-10-05025.1

Butler, A. H., Thompson, D. W. J., & Heikes, R. (2010). The steady-state atmospheric circulation response to climate change–like thermal forcings in a simple general circulation model. *Journal of Climate*, *23*(13), 3474–3496. https://doi.org/10.1175/2010jcli3228.1

Charney, J. G., & Drazin, P. G. (1961). Propagation of planetary-scale disturbances from lower into upper atmosphere. *Journal of Geophysical Research*, *66*(1), 83–109. https://doi.org/10.1029/JZ066i001p00083

Danabasoglu, G., Lamarque, J.-F., Bacmeister, J., Bailey, D. A., DuVivier, A. K., Edwards, J., et al. (2020). The community Earth system model version 2 (CESM2). *Journal of Advances in Modeling Earth Systems*, *12*, e2019MS001916. https://doi.org/10.1029/2019MS001916

Fasullo, J., & Richter, J. H. (2022). Scenario and model dependence of strategic solar climate intervention in CESM. EGUsphere [preprint]. https://doi.org/10.5194/egusphere-2022-779

Ferraro, A. J., Charlton-Perez, A. J., & Highwood, E. J. (2015). Stratospheric dynamics and midlatitude jets under geoengineering with space mirrors and sulfate and titania aerosols. *Journal of Geophysical Research: Atmospheres*, *120*(2), 414–429. https://doi.org/10.1002/2014jd022734

Fujino, J., Nair, R., Kainuma, M., Masui, T., & Matsuoka, Y. (2006). Multi-gas mitigation analysis on stabilization scenarios using Aim global model, Energy Journal., Vol. Multi-Greenhouse Gas Mitigation and Climate Policy, 343.

Gettelman, A., Mills, M. J., Kinnison, D. E., Garcia, R. R., Smith, A. K., Marsh, D. R., et al. (2019). TheWhole atmosphere community Climate-Model version 6 (WACCM6). *Journal of Geophysical Research: Atmospheres*, *124*(23), 12380–12403. https://doi.org/10.1029/2019JD030943

Haigh, J. D., Blackburn, M., & Day, R. (2005). The response of tropospheric circulation to perturbations in lower-stratospheric temperature. *Journal of Climate*, *18*(17), 3672–3685. https://doi.org/10.1175/jcli3472.1

Hijioka, Y., Matsuoka, Y., Nishimoto, H., Masui, M., & Kainuma, M. (2008). Global GHG emissions scenarios under GHG concentration stabilization targets. *Journal of Global Environment Engineering*, *13*, 97–108.

Jones, A., Haywood, J. M., Scaife, A. A., Boucher, O., Henry, M., Kravitz, B., et al. (2022). The impact of stratospheric aerosol intervention on the north Atlantic and quasi-biennial oscillations in the geoengineering model intercomparison project (GeoMIP) G6sulfur experiment. *Atmospheric Chemistry and Physics*, *22*(5), 2999–3016. https://doi.org/10.5194/acp-22-2999-2022

Kang, S. M., Polvani, L. M., Fyfe, J. C., & Sigmond, M. (2011). Impact of polar ozone depletion on subtropical precipitation. *Science*, *332*(6032), 951–954. https://doi.org/10.1126/science.1202131

Kravitz, B., MacMartin, D. G., Mills, M. J., Richter, J. H., Tilmes, S., Lamarque, J.-F., et al. (2017). First simulations of designing stratospheric sulfate aerosol geoengineering to meet multiple simultaneous climate objectives. *Journal of Geophysical Research: Atmospheres*, *122*(23), 12616–12634. https://doi.org/10.1002/2017JD026874

Kravitz, B., MacMartin, D. G., Tilmes, S., Richter, J. H., Mills, M. J., Cheng, W., et al. (2019). Comparing surface and stratospheric impacts of geoengineering with different SO$_2$ injection strategies. *Journal of Geophysical Research: Atmospheres*, *124*(14), 7900–7918. https://doi.org/10.1029/2019jd030329

Liu, X., Ma, P.-L., Wang, H., Tilmes, S., Singh, B., Easter, R. C., et al. (2016). Description and evaluation of a new four mode version of the modal aerosol Module (MAM4) within version 5.3 of the community atmosphere model. *Geoscientific Model Development*, *9*(2), 505–522. https://doi.org/10.5194/gmd-9-505-2016

Lorenz, D. J., & DeWeaver, E. T. (2007). Tropopause height and zonal wind response to global warming in the IPCCscenario integrations. *Journal of Geophysical Research*, *112*(D10), D10119. https://doi.org/10.1029/2006JD008087

MacMartin, D. G., Kravitz, B., Tilmes, S., Richter, J. H., Mills, M. J., Lamarque, J.-F., et al. (2017). The climate response to stratospheric aerosol geoengineering can be tailored using multiple injection locations. *Journal of Geophysical Research: Atmospheres*, *122*(23), 12574–12590. https://doi.org/10.1002/2017JD026868

MacMartin, D. G., Visioni, D., Kravitz, B., Richter, J., Felgenhauer, T., Lee, W. R., et al. (2022). Scenarios for modeling solar radiation modification. *Proceedings of the National Academy of Sciences*, *119*(33). https://doi.org/10.1073/pnas.2202230119

McCusker, K. E., Battisti, D. S., & Bitz, C. M. (2015). Inability of stratospheric sulfate aerosol injections to preserve the West Antarctic ice sheet. *Geophysical Research Letters*, *42*(12), 4989–4997. https://doi.org/10.1002/2015GL064314

McLandress, C., Shepherd, T. G., Scinocca, J. F., Plummer, D. A., Sigmond, M., Jonsson, A. I., & Reader, M. C. (2011). Separating the dynamical effects of climate change and ozone depletion. Part II: Southern hemisphere troposphere. *Journal of Climate*, *24*(6), 1850–1868. https://doi.org/10.1175/2010jcli3958.1

Meinshausen, M., Nicholls, Z. R. J., Lewis, J., Gidden, M. J., Vogel, E., Freund, M., et al. (2020). The shared socio-economic pathway (SSP) greenhouse gas concentrations and their extensions to 2500. *Geoscientific Model Development*, *13*(8), 3571–3605. https://doi.org/10.5194/gmd-13-3571-2020

Polvani, L. M., Waugh, D. W., Correa, G. J. P., & Son, S.-W. (2011). Stratospheric ozone depletion: The main driver of twentieth century atmospheric circulation changes in the Southern Hemisphere? *Journal of Climate*, *24*(3), 210–227. https://doi.org/10.1175/2010jcli3772.1

Richter, J., Visioni, D., MacMartin, D., Bailey, D., Rosenbloom, N., Lee, W., et al. (2022). Assessing Responses and Impacts of Solar climate intervention on the Earth system with stratospheric aerosol injection (ARISE-SAI). EGUsphere [preprint]. https://doi.org/10.5194/egusphere-2022-125

Simpson, I., Tilmes, S., Richter, J., Kravitz, B., MacMartin, D., Mills, M., et al. (2019). The regional hydroclimate response to stratospheric sulfate geoengineering and the role of stratospheric heating. *Journal of Geophysical Research: Atmospheres*, *124*(23), 2019JD031093. https://doi.org/10.1029/2019jd031093

Simpson, I. R., Blackburn, M., & Haigh, J. D. (2009). The role of eddies in driving the tropospheric response to stratospheric heating perturbations. *Journal of the Atmospheric Sciences*, *66*(5), 1347–1365. https://doi.org/10.1175/2008jas2758.1

Son, S. W., Tandon, N. F., Polvani, L. M., & Waugh, D. W. (2009). Ozone hole and Southern Hemisphere climate change. *Geophysical Research Letters*, *36*(5). https://doi.org/10.1029/2009gl038671

Tebaldi, C., Debeire, K., Eyring, V., Fischer, E., Fyfe, J., Friedlingstein, P., et al. (2021). Climate model projections from the scenario model intercomparison project (ScenarioMIP) of CMIP6. *Earth System Dynamics*, *12*(1), 253–293. https://doi.org/10.5194/esd-12-253-2021

Thompson, D. W. J., & Wallace, J. M. (1998). The Arctic oscillation signature in the wintertime geopotential height and temperature fields. *Geophysical Research Letters*, *25*(9), 1297–1300. https://doi.org/10.1029/98GL00950

Thompson, D. W. J., & Wallace, J. M. (2000). Annular modes in the extratropical circulation. Part I: Month-to-Month variability. *Journal of Climate*, *13*(5), 1000–1016. https://doi.org/10.1175/1520-0442(2000)013<1000:amitec>2.0.co;2

Tilmes, S., Richter, J. H., Kravitz, B., MacMartin, D. G., Mills, M. J., Simpson, I. R., et al. (2018). CESM1(WACCM) stratospheric aerosol geoengineering large ensemble project. *Bulletin America Meteorology Social*, *99*(11), 2361–2371. https://doi.org/10.1175/BAMS-D-17-0267.1

Visioni, D., Bednarz, E. M., Lee, W. R., Kravitz, B., Jones, A., Haywood, J. M., & MacMartin, D. G. (2022). Climate response to off-equatorial stratospheric sulfur injections in three Earth system models – Part 1: Experimental protocols and surface changes. EGUsphere [preprint]. https://doi.org/10.5194/egusphere-2022-401